

Frequency comb generation by symmetry-protected bound state in the continuum

KONSTANTIN N. PICHUGIN AND ALMAS F. SADREEV*

L.V. Kirensky Institute of Physics, 660036 Krasnoyarsk, Russia

*Corresponding author: almas@tnp.krasn.ru

Received 17 March 2015; revised 21 May 2015; accepted 16 June 2015; posted 19 June 2015 (Doc. ID 236408); published 16 July 2015

We study the dynamical response of two nonlinear microresonators coupled with a photonic crystal waveguide. We find a domain in the space of frequency and amplitude of the probing light where all stationary solutions are unstable. In this domain, scattered light carries multiple harmonics with equidistantly spaced frequencies [frequency comb (FC) effect]. Two identical resonators coupled with the waveguide support the symmetry-protected bound state in the continuum whose response is singular, as the amplitude of the injected wave tends to zero. As a result, the FC interval tends to zero when the amplitude of probing light diminishes, which paves the way for all-optical generation of waves with ultralow frequency. © 2015 Optical Society of America

OCIS codes: (190.2620) Harmonic generation and mixing; (190.3270) Kerr effect; (350.4238) Nanophotonics and photonic crystals.

<http://dx.doi.org/10.1364/JOSAB.32.001630>

1. INTRODUCTION

Recently, bound states in the continuum (BSC) in photonics have attracted much interest owing to a possibility to localize light in various photonic crystal (PhC) designs [1–15]. BSC is a localized solution of the Maxwell equations that corresponds to a discrete eigenfrequency coexisting with extended modes of continuous spectrum of the PhC waveguide or radiation continuum. The orthogonality of the BSC to accessible continuum channels can be achieved in many ways [8,16], among which the symmetry protection mechanism is the most obvious [2,13–15,17,18]. Arguably, the design of 2D PhC shown in Fig. 1(a), which supports the symmetry-protected BSC, is the simplest. That design was originally proposed in [4] and experimentally implemented by Plotnik *et al.* [5].

Each off-channel defect rod forms an optical microresonator specified by its eigenmodes [19]. In what follows, we assume that only the monopole eigenfrequency resides in the propagation band of the waveguide. Since the system in Fig. 1(a) is symmetrical relative to the waveguide axis, one can classify the eigenmodes of two coupled microresonators as even (symmetric) and odd (antisymmetric) modes. If the propagating mode is symmetrical, the odd eigenmode is decoupled to form a symmetry-protected BSC. For light transmission through the waveguide, the BSC cannot be excited. However, that only holds true until we neglect the nonlinearity of the microcavities due to the Kerr effect. There are a few nonlinear phenomena affecting the BSC and light transmission. First, in nonlinear systems, the principle of linear superposition is not valid, which breaks orthogonality of the BSC to the propagating mode [20]. That results in effective coupling of the odd BSC with the

symmetric propagating mode with the coupling strength dependent on the intensity of light injected into the PhC waveguide. Then, as soon as the BSC becomes a quasi-bound mode, both eigenmodes of the optical microresonators are excited but to a very different extent. Next, in this work, we will show that, for frequencies of injected light close to the frequency of BSC, the quasi-bound state is strongly excited, which provokes instability.

The system of two defect rods form a closed nonlinear quantum dimer, which has attracted much interest [21–27]. The interest is related to the phenomenon of symmetry breaking (self-trapping) [21,22]. On the other hand, nontrivial time-dependent solutions were found for the nonlinear dimer [21–25]. The observation of these remarkable properties of the closed nonlinear dimer implies application of a probing wave, which opens the dimer. Respectively, temporal equations describing the open nonlinear dimer become nonintegrable, which constitutes the main difference between the closed and open nonlinear dimers. Dependency on the way of opening the stationary transmission through a nonlinear dimer was studied in [26,28–35], where the phenomenon of symmetry breaking was reported. It is interesting to note there is a domain in the space of frequency and amplitude of the injected wave where stable stationary solutions of the temporal equations do not exist [34,35]. Thus, one can expect that the dynamical response of the nonlinear dimer will display features that cannot be described by the stationary scattering theory. In particular, injection of a monochromatic symmetric wave into the nonlinear plaquette gives rise to emission of antisymmetric satellite waves with frequencies different from the frequency of the incident wave [35].

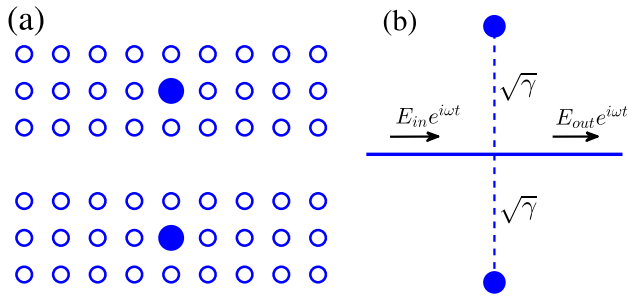


Fig. 1. (a) Two microcavities made from a Kerr media (marked by filled circles) are inserted into the square lattice photonic crystal of dielectric rods. The 1D waveguide is formed by extraction of a linear chain. (b) Two nonlinear sites (marked by filled circles) are positioned symmetrically relative to the waveguide and form an open nonlinear dimer.

This phenomenon is known as frequency comb (FC) generation and is widely studied in various linear and nonlinear systems [36–43]. FC generation has been demonstrated in continuously pumped optical microresonators, exploiting the third-order nonlinear susceptibility. In such Kerr combs, the first couple of side modes are produced through a degenerate four-wave mixing threshold process. These successive cascaded processes eventually lead to a uniform broadband FC. In this paper, we show a similar phenomenon for illumination of the nonlinear dimer in the domain of instability of the open dimer. However, the main result is a possibility to enormously diminish the FC interval Ω due to the symmetry-protected BSC in the open nonlinear dimer.

2. COUPLED MODE THEORY EQUATIONS

Taking that the radii of the rods are small enough, we can present each rod by a single site variable $A_j, j = 1, 2$ disregarding space inhomogeneity of electromagnetic field in the rods. In terms of the eigenfunctions of the Maxwell equations for each microresonator, this means that only the monopole mode with the eigenfrequency ω_0 resides in the PhC waveguide propagation band and, thereby, is relevant in the scattering. For simplicity, we disregard the dispersion properties of the waveguide and write for the dimer illuminated by light with the amplitude E_{in} and frequency ω the following temporal coupled mode theory (CMT) equations [34,44,45]:

$$\begin{aligned} -i\dot{A}_1 &= (\omega_1 + \lambda|A_1|^2)A_1 + uA_2 + i\gamma_1 A_1 \\ &\quad + i\sqrt{\gamma_1\gamma_2}A_2 - i\sqrt{\gamma_1}E_{in}e^{i\omega t}, \\ -i\dot{A}_2 &= (\omega_2 + \lambda|A_2|^2)A_2 + uA_1 + i\sqrt{\gamma_1\gamma_2}A_1 \\ &\quad + i\gamma_2 A_2 - i\sqrt{\gamma_2}E_{in}e^{i\omega t}, \end{aligned} \quad (1)$$

Here, the terms $\lambda|A_j|^2 A_j, j = 1, 2$ account for the Kerr effect of each microresonator; the term $\sqrt{\gamma_j}$ is responsible for the coupling of the j th off-channel resonator with the waveguide. The monopole mode of each resonator is localized within a few lattice units [19] so that $u < \sqrt{\gamma_j}$. In the design shown in Fig. 1(a), the defect rods are positioned at a distance of two lattice units, while the distance between the defect rods equals

four units. Then, overlapping between the monopole modes of the resonators is negligibly small compared with the overlapping between the monopole mode and the waveguide mode, i.e., $u \ll \sqrt{\gamma_j}$. Even for this case, the open nonlinear dimer remains cardinally different from the case of the closed dimer because of the interaction between the cavities via the continuum.

The open dimer governed by the CMT equations [Eq. (1)] is shown in Fig. 1(b). By substituting $A_j(t) = a_j(t) \exp(i\omega t)$, the temporal CMT equations [Eq. (1)] become

$$\begin{aligned} -i\dot{a}_1 &= (\nu_1 + \lambda|a_1|^2)a_1 + i\gamma_1 a_1 + i\sqrt{\gamma_1\gamma_2}a_2 - i\sqrt{\gamma}E_{in}, \\ -i\dot{a}_2 &= (\nu_2 + \lambda|a_2|^2)a_2 + i\sqrt{\gamma_1\gamma_2}a_1 + i\gamma_2 a_2 - i\sqrt{\gamma}E_{in}, \end{aligned} \quad (2)$$

where $\nu_j = \omega_j - \omega$. The amplitude of the transmitted wave is given by the following equation [34,45]:

$$E_{out} = E_{in} - \sqrt{\gamma_1}a_1 - \sqrt{\gamma_2}a_2. \quad (3)$$

3. INSTABILITY OF STATIONARY SOLUTIONS

Numerical analysis of stability of the stationary solutions revealed a domain in the space of parameters ω and E_{in} , where *all* stationary solutions are unstable [34]. A similar result was found in the open plaquette of four nonlinear sites [35]. In this section, we find the domain of instability of stationary solutions of temporal equations [Eq. (1)]. To examine the stability of the solutions in Eq. (2), we apply a standard small perturbation technique [46]:

$$a_j(t) = a_{j0} + (x_j + iy_j)e^{\mu t}, \quad j = 1, 2, \quad (4)$$

where the second term in Eq. (4) is considered to be small. The domain of instability defined by the condition $\mu = 0$ was evaluated numerically and is shaded, as shown in Fig. 2, in blue. One can see a threshold in the amplitude of the injected wave E_{in} .

For the symmetric nonlinear dimer $\nu_j = \nu, \gamma_j = \gamma$, the domain of instability can be evaluated analytically. For the

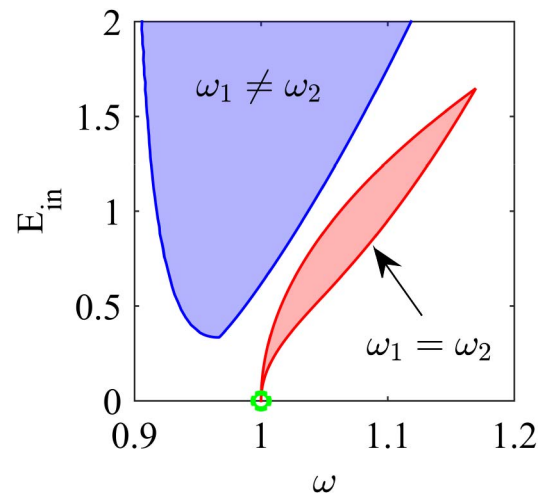


Fig. 2. Instability domains in space of physical parameters ω and E_{in} . The nonsymmetric case with $\omega_1 = 1, \omega_2 = 0.9, \gamma_1 = \gamma_2 = \gamma$ is shown in blue. The symmetric case $\omega_1 = \omega_2$ is shown in red. The BSC point is shown by an open green circle. Other parameters are $\omega_0 = 1, \gamma = 0.04, \lambda = 0.01, u = 0$.

stationary symmetry preserved stationary solution, we have from Eq. (2) [34]

$$a_{10} = a_{20} = a_0 = \frac{i\sqrt{\gamma}E_{\text{in}}}{\nu + u + \lambda I_0 + 2i\gamma}, \quad (5)$$

where, according to Eq. (1),

$$I_0[(\nu + u + \lambda I_0)^2 + 4\gamma^2] = \gamma E_{\text{in}}^2, \quad (6)$$

and $I_0 = |a_0|^2$. Substituting Eq. (4) into Eq. (2), we obtain the following system of algebraic equations:

$$\begin{aligned} & -(\mu + 2\gamma + 2\lambda \text{Re}(a_0)\text{Im}(a_0))(x_1 + x_2) \\ & = (\nu + u + \lambda I_0 + 2\lambda \text{Im}(a_0)^2)(y_1 + y_2) \\ & \quad \times (\mu + 2\gamma - 2\lambda \text{Re}(a_0)\text{Im}(a_0))(y_1 + y_2) \\ & = (\nu + u + \lambda I_0 + 2\lambda \text{Re}(a_0)^2)(x_1 + x_2), \end{aligned} \quad (7)$$

and

$$\begin{aligned} & -(\mu + 2\lambda \text{Re}(a_0)\text{Im}(a_0))(x_1 - x_2) \\ & = (\nu - u + \lambda I_0 + 2\lambda \text{Im}(a_0)^2)(y_1 - y_2), \\ & \quad \times (\mu + 2\lambda \text{Re}(a_0)\text{Im}(a_0))(y_1 - y_2) \\ & = (\nu - u + \lambda I_0 + 2\lambda \text{Re}(a_0)^2)(x_1 - x_2). \end{aligned} \quad (8)$$

Using the eigenmode variables (symmetric and antisymmetric),

$$a_{s,a} = \frac{1}{2}(a_1 \pm a_2), \quad \nu_{s,a} = \nu \pm u, \quad (9)$$

one can see that Eq. (7) describes the symmetric oscillations, while Eq. (8) does the antisymmetric oscillations around the symmetric stationary state; more importantly, these oscillations are separated. For the symmetric oscillations, we have from Eq. (7) the eigenvalues

$$\mu_s = -2\gamma \pm i\sqrt{(\nu + u + \lambda I_0)(\nu + 3\lambda I_0)}. \quad (10)$$

Equation $\mu_s = 0$ defines the boundary of instability of the symmetrical stationary solution relative to the symmetric perturbation. This instability is typical for the single nonlinear resonator [19]. Owing to a contribution -2γ in Eq. (10), instability occurs at a finite value of the injected amplitude E_{in} [34]. Equation (8) for the antisymmetric perturbations has the following eigenvalues,

$$\mu_a^2 = -(\nu - u + \lambda I_0)(\nu - u + 3\lambda I_0), \quad (11)$$

and gives the boundary of stability, $\nu - u + \lambda I_c = 0$ and $\nu - u + 3\lambda I_c = 0$. Substituting these values of I_c into Eq. (6), we obtain for the boundaries of the domain where the stationary symmetric solution is destabilized by antisymmetric oscillations:

$$\begin{aligned} E_{\text{in}}^2 &= -\frac{4(\gamma^2 + u^2)(\nu - u)}{\gamma\lambda}, \\ E_{\text{in}}^2 &= -\frac{4(\nu - u)}{3\gamma\lambda}[(\nu + 2u)^2/9 + \gamma^2]. \end{aligned} \quad (12)$$

Different from the nonsymmetric dimer, the domain of instability of the symmetric dimer emerges from the point $E_{\text{in}} = 0$, $\omega = \omega_a = \omega_0 - u$, which is exactly the BSC point. Without loss of generality, we can take $u = 0$ with the instability domain, as shown in Fig. 2 in red. Since all stationary solutions

are unstable in this domain, one can expect a generation of harmonics with the frequency interval between them $\Omega \sim E_{\text{in}}^2$. In what follows, we focus on the case of the symmetric dimer with $u = 0$. Rigorously speaking, the true BSC with a zero resonant width in nonlinear system exists at the point marked by open green circle in Fig. 2 [20]. Nevertheless, we can conclude that the BSC excitations play a crucial role in the stability of the symmetric dimer, at least, for small injected amplitudes.

4. NUMERICAL SOLUTIONS OF NONLINEAR TEMPORAL CMT EQUATIONS

One can see from Eq. (2) for the identical microresonators that the solutions possess a symmetry with the half-period time shift corresponding to the permutation of the sites:

$$a_1(t + T/2) = a_2(t), \quad a_2(t + T/2) = a_1(t). \quad (13)$$

Indeed, after time shift $t \rightarrow t + T/2$ in the first equation in Eq. (2), we obtain the second equation using Eq. (13) and the periodicity of the solutions. Thus, the system of Eq. (2) is reduced to one temporal equation:

$$\begin{aligned} -i\dot{a}_j &= (\nu + \lambda|a_j(t)|^2)a_j(t) + i\gamma(a_j(t) + a_j(t + T/2)) \\ & \quad - i\sqrt{\gamma}E_{\text{in}}. \end{aligned} \quad (14)$$

Nevertheless, the symmetry in Eq. (13) does not allow us to solve Eq. (14) because of unknown period T , which strongly depends on the intensity of the injected wave. In Figs. 3 and 4, we present the results of numerical simulations of Eq. (2) in the domain of unstable stationary solutions, which demonstrate the symmetry in Eq. (13). Figure 4 also demonstrates the ratchet effect due to the absence of the time reversal symmetry in the open dimer. We chose the parameters listed in the caption of Figs. 3 and 4 guided by the data on PhC microcavities from [34].

In order to compare the results with the closed dimer in [21], we present trajectories projected onto the modulus $|a_j|$ and phase difference $\Delta\theta$ between cavities in Fig. 5(a). Although for a small injected amplitude E_{in} , the trajectories look similar to those shown in [21], with the growth of E_{in} the trajectories become asymmetrical relative to $\Delta\theta \rightarrow -\Delta\theta$. The trajectories projected onto the real and imaginary parts of the amplitudes $a_j(t)$ demonstrate the most striking difference between the closed and open nonlinear dimer, as shown in Fig. 5(b). While for the closed dimer the trajectories form circles centered at the origin of the coordinate system [they

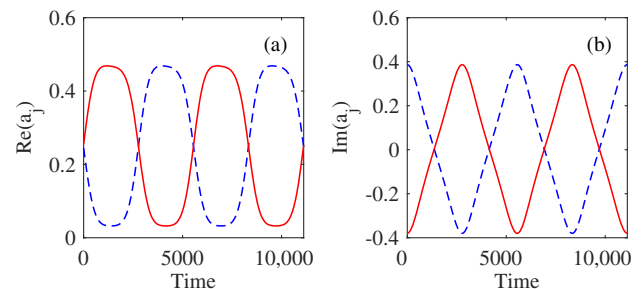


Fig. 3. Time evolution of site amplitudes $a_j(t)$, $j = 1, 2$, real and imaginary parts for $E_{\text{in}} = 0.1$, $\nu = -0.001$, $\gamma = 0.04$, $\lambda = 0.01$.

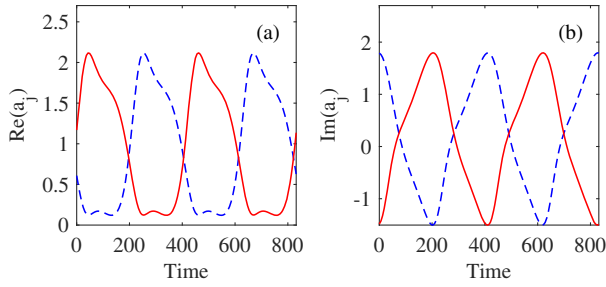


Fig. 4. Same as in Fig. 3 but for the parameters $E_{\text{in}} = 0.4$, $\nu = -0.02$, $\gamma = 0.04$, $\lambda = 0.01$.

are not shown in Fig. 5(b)], the trajectories of the open dimer are shifted relative to the coordinate origin. Phase transformation of the injected wave $E_{\text{in}} \rightarrow E_{\text{in}}e^{i\alpha}$ rotates the trajectories in Fig. 5(b) by the same angle α .

It is clear that such a complicated time behavior of the amplitudes will reflect at the transmitted wave, according to Eq. (3). Figure 6 shows the Fourier transformation of the transmitted wave:

$$E_{\text{out}}(t) = \int E_{\text{out}}(f) \exp(ift) df, \quad (15)$$

which demonstrates sharp peaks spaced equidistantly, i.e., the FC comb effect. In what follows, we define the interval between the peaks of the Fourier transform $F_{\text{out}}(f)$ as the FC interval Ω . One can see from Fig. 6 that $|E_{\text{out}}(f)| \neq |E_{\text{out}}(-f)|$, which is a consequence of the ratchet effect, as seen in Fig. 4. In Fig. 6, we present results for the nonsymmetric dimer (a) and the symmetric dimer (b), which both demonstrate the FC effect. However, only for the last case, the FC frequency interval Ω can be limited to zero due to the BSC participation in the wave transmission through the symmetric nonlinear dimer.

5. ASYMPTOTIC EVALUATION OF THE FC INTERVAL

The reason for the cardinal difference between the closed and open nonlinear dimers is the symmetry of the system. Let us rewrite Eq. (2) in terms of the eigenmodes of the closed linear dimer:

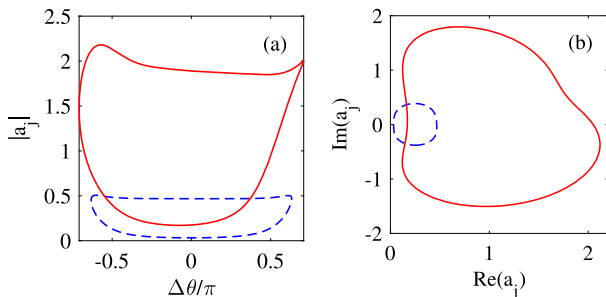


Fig. 5. (a) Trajectories projected onto $|a_j|$ and phase difference $\Delta\theta = \theta_1 - \theta_2$ and (b) real and imaginary parts of amplitudes $a_j(t)$, $j = 1, 2$ for different points in the domain of instability: $E_{\text{in}} = 0.1$, $\nu = -0.001$ (blue dashed line) and $E_{\text{in}} = 0.4$, $\nu = -0.02$ (red solid line). Other parameters are $\omega_0 = 1$, $\gamma = 0.04$, $\lambda = 0.01$.

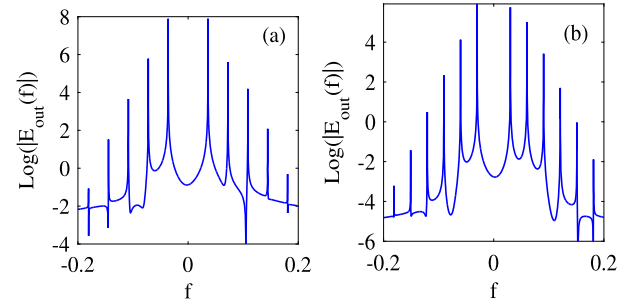


Fig. 6. Fourier transform $E_{\text{out}}(f)$ of the transmitted wave in log scale. (a) Nonsymmetric dimer with $\omega_1 = 1$, $\omega_2 = 0.9$. (b) Symmetric dimer with $\omega_1 = \omega_2 = \omega_0 = 1$. Other parameters are listed in Fig. 4.

$$\begin{aligned} -i\dot{a}_s &= (\nu + \lambda[|a_s|^2 + 2|a_a|^2])a_s + \lambda a_a^2 a_s^* + 2i\gamma a_s - i\sqrt{\gamma}E_{\text{in}}, \\ -i\dot{a}_a &= (\nu + \lambda[|a_a|^2 + 2|a_s|^2])a_a + \lambda a_s^2 a_a^*, \end{aligned} \quad (16)$$

where the modes $a_{s,a}$ with the eigenfrequencies $\omega_{s,a} = \omega_0$ are defined in Eq. (9).

Let us assume temporarily the dimer is linear. The design of the open dimer (Fig. 1) implies that the injected wave can probe only the symmetric mode with a Breit–Wigner response $a_s = i\sqrt{\gamma}E_{\text{in}}/(\nu + 2i\gamma)$, while the antisymmetric mode remains hidden, as seen from the CMT equations [Eq. (16)]. It oscillates with the frequency ν but with the uncertain amplitude a , which defines the antisymmetric mode as a symmetry-protected BSC [4,5,8]. Returning to the site amplitudes, we have

$$a_j = \frac{i\sqrt{\gamma}E_{\text{in}}}{\nu + 2i\gamma} \pm ae^{i\nu t}, \quad j = 1, 2, \quad (17)$$

which makes the time behavior of the site amplitudes of the linear dimer nonstationary. This equation constitutes the time-dependent contribution of the bound state in the continuum established for the stationary case in quantum mechanical [47] and PhC systems [4].

The nonlinearity results in two effects. The first obvious result is that the resonance eigenfrequency $\nu + \lambda I_0$ of the symmetric mode is shifted proportional to E_{in}^2 , which agrees with the instability domain at small E_{in} , as derived in Section 3 and shown in Fig. 2. The second effect is more sophisticated. For small E_{in} , the symmetric mode a_s is almost constant while oscillations of the antisymmetric mode a_a are dominant, as shown in Fig. 7. That result is an obvious effect of the symmetry-protected BSC whose response tends to be infinite when $E_{\text{in}} \rightarrow 0$ because of zero resonant width at $E_{\text{in}} = 0$. As seen from the first equation in Eq. (16), the antisymmetric mode plays the role of a driving force for the mode a_s via the nonlinear term $\lambda a_a^2 a_s^*$. If the frequency of the mode a_a is Ω , then the symmetric mode oscillates with double frequency 2Ω , as is seen in the numerical solution in Fig. 7. Respectively, the transmitted wave carries the harmonics with the same frequency 2Ω in accordance with Eq. (3).

In order to consider these nonlinear effects quantitatively, we use the asymptotic methods by Bogoliubov and Mitropolsky [48]. Equation (16) can be rewritten as follows:

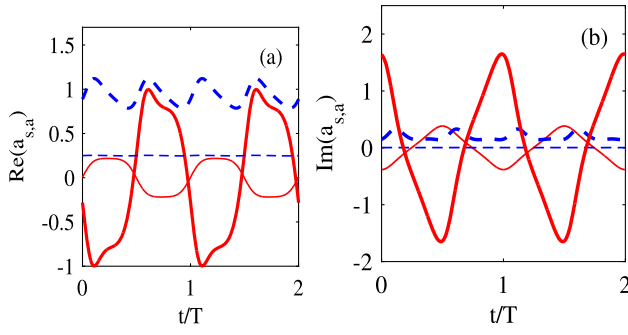


Fig. 7. Time evolution of real parts (a) and imaginary parts (b) of symmetric (blue dashed lines) and antisymmetric mode (red solid lines) for $E_{\text{in}} = 0.1$, $\nu = -0.001$ (thin lines) and $E_{\text{in}} = 0.2$, $\nu = -0.02$ (thick lines). Other parameters are $\omega_0 = 1$, $\gamma = 0.04$, $\lambda = 0.01$.

$$\begin{aligned} i\dot{a}_s + (\nu + 2i\gamma)a_s - i\sqrt{\gamma}E_{\text{in}} &= \varepsilon F_s(a_s, a_a), \\ i\dot{a}_a + \nu a_a &= \varepsilon F_a(a_s, a_a), \end{aligned} \quad (18)$$

where λ is considered a small parameter ε and functions $F_{s,a}$ are polynomial functions of $a_{s,a}$ determined by Eq. (16). Then, the solution up to the first order in ε can be sought in the form

$$a_s = s_0(a, \phi) + \varepsilon s_1(a, \phi), \quad a_a = a_0(a, \phi) + \varepsilon a_1(a, \phi), \quad (19)$$

as functions of the amplitude a and phase ϕ . They are given by the following equations:

$$\dot{a} = \varepsilon D_1(a), \quad \dot{\phi} = \nu + \varepsilon \Omega_1(a), \quad (20)$$

where ν is the frequency of oscillations at $\varepsilon = 0$. Substitution of Eqs. (19) and (20) and the relation

$$\dot{a}_{s,a} = \dot{a} \frac{\partial a_{s,a}}{\partial a} + \dot{\phi} \frac{\partial a_{s,a}}{\partial \phi} \quad (21)$$

into Eq. (16) gives the following equation at the zeroth order in parameter ε :

$$s_0(a, \phi) = \frac{i\sqrt{\gamma}E_{\text{in}}}{\nu + 2i\gamma}, \quad a_0(a, \phi) = a \exp(i\phi), \quad (22)$$

where the amplitude a is undefined.

In the first order in ε , we obtain the following equations:

$$\begin{aligned} -i\nu \frac{\partial s_1}{\partial \phi} &= (\nu + 2i\gamma)s_1 + a_0^2 s_0^* + (|s_0|^2 + 2a^2)s_0, \\ -i\nu \frac{\partial a_1}{\partial \phi} &= \nu a_1 + s_0^2 a_0^* + (a^2 + 2|s_0|^2)a_0 + (iD_1 - a\Omega_1) \exp(i\phi). \end{aligned} \quad (23)$$

One can expand

$$\begin{aligned} s_1(a, \phi) &= \sum_n F_{s,n}(a) \exp(in\phi), \\ a_1(a, \phi) &= \sum_n F_{a,n}(a) \exp(in\phi). \end{aligned} \quad (24)$$

According to [48], there is uncertainty in the choice of functions s_1 and a_1 , which allows us to exclude, for example, the first harmonic contributions $F_{s,1}$, $F_{a,1}$, which give the following equations:

$$D_1(a) = 0, \quad \Omega_1(a) = a^2 + 2|s_0|^2. \quad (25)$$

Then, solutions of Eq. (23) are as follows:

$$\begin{aligned} s_1(a, \phi) &= -\frac{|s_0|^2 + 2a^2}{\nu + 2i\gamma} s_0 + \frac{a^2}{\nu - 2i\gamma} s_0^* \exp(2i\phi), \\ a_1(a, \phi) &= -\frac{a}{2\nu} s_0^2 \exp(-i\phi). \end{aligned} \quad (26)$$

This equations show that the symmetric solution consists of even terms $n = 0, \pm 2, \dots$ in Eq. (24), while the antisymmetric solution consists of the odd terms $n = \pm 1, \pm 3, \dots$. The higher orders in the small parameter preserve the same features. From Eq. (20), we have

$$\dot{\phi} = (\nu + \lambda(a^2 + 2|s_0|^2))t = \Omega_a t, \quad (27)$$

which yields the FC interval $\Omega_{\text{FC}} = 2\Omega_a$ in the first order in λ with the amplitude a remaining undefined. This amplitude can be determined by the equation $\dot{a} = 0$ in Eq. (20) if the injected amplitude E_{in} is taken as a small parameter ε in the perturbation approach. However, that approach is successful only in the fourth order in ε , resulting in cumbersome equations. Therefore, we estimate the amplitude a averaging the numerical solution over time: $a = \langle a_a(t) \rangle$. The numerical result shown in Fig. 8(a) is close to the analytical result [Eq. (27)] in Fig. 8(b) when the injected amplitude is small. Thus, the FC interval between harmonics generated by the open nonlinear dimer can be effectively controlled by the injected amplitude.

It is surprising that the FC effect with the FC interval Ω emerging from the BSC point, as shown in Fig. 8, is preserved even for different couplings $\gamma_j, j = 1, 2$ but for $\omega_1 = \omega_2$. By linear transformation,

$$a_s = \sqrt{\gamma_1} a_1 + \sqrt{\gamma_2} a_2, \quad a_a = \frac{a_1}{\sqrt{\gamma_1}} - \frac{a_2}{\sqrt{\gamma_2}}, \quad (28)$$

with

$$a_1 = \frac{\sqrt{\gamma_1}}{\gamma_1 + \gamma_2} (a_s + \gamma_2 a_a), \quad a_2 = \frac{\sqrt{\gamma_2}}{\gamma_1 + \gamma_2} (a_s - \gamma_1 a_a). \quad (29)$$

Equation (2) takes the following form:

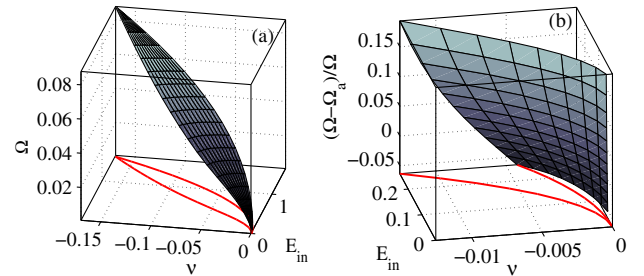


Fig. 8. (a) FC interval between harmonics Ω versus amplitude E_{in} and frequency ν of injected monochromatic wave calculated numerically. (b) Difference between numerical data and analytical results given by Eq. (27). Parameters of the dimer are $\omega_0 = 1$, $\gamma = 0.01$, $\lambda = 0.01$. Below the domain of instability defined by Eq. (12) is shown by red lines.

$$\begin{aligned}
-i\dot{a}_s &= \nu a_s + \lambda \left[\frac{\gamma_1^2}{(\gamma_1 + \gamma_2)^3} |a_s + \gamma_2 a_a|^2 (a_s + \gamma_2 a_a) \right. \\
&\quad \left. + \frac{\gamma_2^2}{(\gamma_1 + \gamma_2)^3} |a_s - \gamma_1 a_a|^2 (a_s - \gamma_1 a_a) \right] + i(\gamma_1 + \gamma_2)(a_s - E_{\text{in}}), \\
-i\dot{a}_a &= \nu a_a + \lambda \left[\frac{\gamma_1}{(\gamma_1 + \gamma_2)^3} |a_s + \gamma_2 a_a|^2 (a_s + \gamma_2 a_a) \right. \\
&\quad \left. - \frac{\gamma_2}{(\gamma_1 + \gamma_2)^3} |a_s - \gamma_1 a_a|^2 (a_s - \gamma_1 a_a) \right]. \tag{30}
\end{aligned}$$

One can see that, similar to the former symmetric case $\gamma_1 = \gamma_2$, the mode a_a is coupled with the injected wave only through the nonlinear terms.

6. SUMMARY AND DISCUSSION

In this paper, we considered one of the simplest nonlinear open systems: the nonlinear dimer whose closed counterpart is an integrable system [21]. The term “open” means that a linear waveguide is attached to the dimer to allow probing its dynamical properties. Even in the case of decoupled nonlinear sites, they interact with each other through the continuum of the waveguide. In the framework of CMT, we examined the stability of stationary solutions of Eq. (1) in the parametric space of frequency and amplitude of the probing wave. We found a domain where *all* stable stationary solutions do not exist. First, such domains were found in open nonlinear plaquette [35] together with the associated effect of FC generation. In the present paper, we showed a similar FC effect for the scattering of a monochromatic wave by a nonlinear dimer. The nature of the FC is the side harmonics produced through a degenerate four-wave-mixing threshold process, which has been well studied, theoretically and experimentally [38–42]. For the different microresonators, numerics show a similar threshold relative to the amplitude of the injected monochromatic wave, as shown in Fig. 2 in blue.

The identical microresonators with the Kerr effect symmetrically coupled with a waveguide represent a unique case when this threshold tends zero if the frequency of the injected wave approaches the eigenfrequency of the microresonators. This phenomenon is related to a symmetry-protected BSC. When the dimer is linear, there are two eigenmodes: symmetric and antisymmetric. The symmetrical design of opening of the dimer (see Fig. 1) implies that the injected wave couples only with the symmetric mode, while there is no direct coupling of the injected wave with the antisymmetric mode transforming it into the symmetry-protected BSC [4,5]. However, owing to nonlinear terms in Eq. (16), the antisymmetric mode a_a is coupled with an injected wave through the symmetric mode a_s . Therefore, the BSC emerges in the response in the vicinity of the resonance $\omega = \omega_0$. This effects gives rise to the FC generation of side harmonics with the frequency interval $\Omega \sim E_{\text{in}}^2$, as Fig. 8 shows, provided that the frequency and amplitude fall within the instability domain, shown in Fig. 2 in red. Therefore, participation of the symmetry-protected BSC in the nonstationary transmission of monochromatic light by two symmetric off-channel microresonators leads to generation of extremely low-frequency harmonics effectively manipulated

by the injected light amplitude. That result promises important applications of the effect of BSC in photonic systems.

The numerical solution of the temporal CMT equations [Eq. (16)] demonstrates highly nonlinear behavior of the site amplitudes, which are cardinaly different from the dynamical behavior of the closed dimer in the instability domain. Time dependence of these amplitudes holds many harmonics whose frequencies are equidistantly spaced with the interval Ω . This interval, which defines the FC interval, was computed numerically and evaluated by the use of asymptotic methods [48] to demonstrate an agreement, as shown in Fig. 8. Respectively, the injected wave after scattering by the nonlinear dimer acquires side harmonics. Owing to symmetry-protected BSC, the FC interval Ω can become extremely small for approaching the BSC point. Thus, the system of two microresonators with the Kerr effect positioned beside the PhC waveguide opens the way of conversion of input optical signals into terahertz outputs.

Funding. Russian Foundation for Basic Research (RFBR) (03-02-00497).

Acknowledgment. A. F. Sadreev deeply acknowledges fruitful discussions with L. S. Cao regarding the problems with frequency combs. The authors also thank D. N. Maksimov and V. V. Val'kov.

REFERENCES

1. S. Fan, P. R. Villeneuve, J. D. Joannopoulos, M. J. Khan, C. Manolatou, and H. A. Haus, “Theoretical analysis of channel drop tunneling processes,” *Phys. Rev. B* **59**, 15882–15892 (1999).
2. S. P. Shipman and S. Venakides, “Resonant transmission near non-robust periodic slab modes,” *Phys. Rev. E* **71**, 026611 (2005).
3. D. C. Marinica, A. G. Borisov, and S. V. Shabanov, “Bound states in the continuum in photonics,” *Phys. Rev. Lett.* **100**, 183902 (2008).
4. E. N. Bulgakov and A. F. Sadreev, “Bound states in the continuum in photonic waveguides inspired by defects,” *Phys. Rev. B* **78**, 075105 (2008).
5. Y. Plotnik, O. Peleg, F. Dreisow, M. Heinrich, S. Nolte, A. Szameit, and M. Segev, “Experimental observation of optical bound states in the continuum,” *Phys. Rev. Lett.* **107**, 183901 (2011).
6. G. Corrielli, G. Della Valle, A. Crespi, R. Osellame, and S. Longhi, “Observation of surface states with algebraic localization,” *Phys. Rev. Lett.* **111**, 220403 (2013).
7. S. Weimann, Y. Xu, R. Keil, A. E. Miroshnichenko, A. Tunnermann, S. Nolte, A. A. Sukhorukov, A. Szameit, and Y. S. Kivshar, “Compact surface Fano states embedded in the continuum of waveguide arrays,” *Phys. Rev. Lett.* **111**, 240403 (2013).
8. C. W. Hsu, B. Zhen, S.-L. Chua, S. G. Johnson, J. D. Joannopoulos, and M. Soljačić, “Bloch surface eigenstates within the radiation continuum,” *Light Sci. Appl.* **2**, e84 (2013).
9. C. W. Hsu, B. Zhen, J. Lee, S.-L. Chua, S. G. Johnson, J. D. Joannopoulos, and M. Soljačić, “Observation of trapped light within the radiation continuum,” *Nature* **499**, 188–191 (2013).
10. E. N. Bulgakov and A. F. Sadreev, “Robust bound state in the continuum in a nonlinear microcavity embedded in a photonic crystal waveguide,” *Opt. Lett.* **39**, 5212–5215 (2014).
11. Y. Yang, C. Peng, Y. Liang, Z. Li, and S. Noda, “Analytical perspective for bound states in the continuum in photonic crystal slabs,” *Phys. Rev. Lett.* **113**, 037401 (2014).
12. B. Zhen, C. W. Hsu, L. Lu, A. D. Stone, and M. Soljačić, “Topological nature of bound states in the radiation continuum,” *Phys. Rev. Lett.* **113**, 257401 (2014).

13. E. N. Bulgakov and A. F. Sadreev, "Bloch bound states in the radiation continuum in a periodic array of dielectric rods," *Phys. Rev. A* **90**, 053801 (2014).
14. M. Song, H. Yu, C. Wang, N. Yao, M. Pu, J. Luo, Z. Zhang, and X. Luo, "Sharp Fano resonance induced by a single layer of nanorods with perturbed periodicity," *Opt. Express* **23**, 2895–2903 (2015).
15. M. Zhang and X. Zhang, "Ultrasensitive optical absorption in graphene based on bound states in the continuum," *Sci. Rep.* **5**, 8266 (2015).
16. E. N. Bulgakov and A. F. Sadreev, "Formation of bound states in the continuum for a quantum dot with variable width," *Phys. Rev. B* **83**, 235321 (2011).
17. N. Moiseyev, "Suppression of Feshbach resonance widths in two-dimensional waveguides and quantum dots: a lower bound for the number of bound states in the continuum," *Phys. Rev. Lett.* **102**, 167404 (2009).
18. J. Mur-Petit and R. A. Molina, "Chiral bound states in the continuum," *Phys. Rev. B* **90**, 035434 (2014).
19. J. Joannopoulos, R. D. Meade, and J. Winn, *Photonic Crystals* (Princeton University, 1995).
20. E. N. Bulgakov and A. F. Sadreev, "Bound states in photonic Fabry–Perot resonator with nonlinear off-channel defects," *Phys. Rev. B* **81**, 115128 (2010).
21. J. C. Eilbeck, P. S. Lomdahl, and A. C. Scott, "The discrete self-trapping equation," *Phys. D* **16**, 318–338 (1985).
22. V. M. Kenkre and D. K. Campbell, "Self-trapping on a dimer: time-dependent solutions of a discrete nonlinear Schrödinger equation," *Phys. Rev. B* **34**, 4959–4961 (1986).
23. G. P. Tsironis and V. M. Kenkre, "Initial condition effects in the evolution of a nonlinear dimer," *Phys. Lett. A* **127**, 209–212 (1988).
24. V. M. Kenkre and H.-L. Wu, "Time evolution of the nonadiabatic nonlinear quantum dimer," *Phys. Rev. B* **39**, 6907–6913 (1989).
25. G. P. Tsironis, W. D. Deering, and M. I. Molina, "Applications of self-trapping in optically coupled devices," *Phys. D* **68**, 135–137 (1993).
26. A. E. Miroshnichenko, B. A. Malomed, and Y. S. Kivshar, "Nonlinearly-PT-symmetric systems: spontaneous symmetry breaking and transmission resonances," *Phys. Rev. A* **84**, 012123 (2011).
27. H. Xu, P. G. Kevrekidis, and A. Saxena, "Generalized dimers and their Stokes-variable dynamics," *J. Phys. A* **48**, 055101 (2015).
28. B. Maes, M. Soljačić, J. D. Joannopoulos, P. Bienstman, R. Baets, S.-P. Gorza, and M. Haelterman, "Switching through symmetry breaking in coupled nonlinear micro-cavities," *Opt. Express* **14**, 10678–10683 (2006).
29. B. Maes, P. Bienstman, and R. Baets, "Symmetry breaking with coupled Fano resonances," *Opt. Express* **16**, 3069–3076 (2008).
30. A. E. Miroshnichenko, "Nonlinear Fano–Feshbach resonances," *Phys. Rev. E* **79**, 026611 (2009).
31. V. A. Brazhnyi and B. A. Malomed, "Spontaneous symmetry breaking in Schrödinger lattices with two nonlinear sites," *Phys. Rev. A* **83**, 053844 (2011).
32. Y. Xu and A. E. Miroshnichenko, "Reconfigurable nonreciprocity with a nonlinear Fano diode," *Phys. Rev. B* **89**, 134306 (2014).
33. I. V. Barashenkov, G. S. Jackson, and S. Falch, "Blow-up regimes in the PT-symmetric coupler and the actively coupled dimer," *Phys. Rev. A* **88**, 053817 (2013).
34. E. N. Bulgakov, K. N. Pichugin, and A. F. Sadreev, "Symmetry breaking for transmission in a photonic waveguide coupled with two off-channel nonlinear defects," *Phys. Rev. B* **83**, 045109 (2011).
35. D. N. Maksimov and A. F. Sadreev, "Symmetry breaking in binary chains with nonlinear sites," *Phys. Rev. E* **88**, 032901 (2013).
36. P. Del'Haye, A. Schliesser, O. Arcizet, T. Wilken, R. Holzwarth, and T. J. Kippenberg, "Optical frequency comb generation from a monolithic microresonator," *Nature* **450**, 1214–1217 (2007).
37. T. J. Kippenberg, R. Holzwarth, and S. A. Diddams, "Microresonator-based optical frequency combs," *Science* **332**, 555–559 (2011).
38. A. B. Matsko, A. A. Savchenkov, W. Liang, V. S. Ilchenko, D. Seidel, and L. Maleki, "Mode-locked Kerr frequency combs," *Opt. Lett.* **36**, 2845–2847 (2011).
39. M. Foster, J. S. Levy, O. Kuzucu, K. Saha, M. Lipson, and A. L. Gaeta, "Silicon-based monolithic optical frequency comb source," *Opt. Express* **19**, 14233–14239 (2011).
40. L. S. Cao, D. X. Qi, R. W. Peng, M. Wang, and P. Schmelcher, "Phononic frequency combs via nonlinear resonances," *Phys. Rev. Lett.* **112**, 075505 (2014).
41. D. M. Abrams, A. Slawik, and K. Srinivasan, "Nonlinear oscillations and bifurcations in silicon photonic microresonators," *Phys. Rev. Lett.* **112**, 123901 (2014).
42. I. Ricciardi, S. Mosca, M. Parisi, P. Maddaloni, L. Santamaria, P. De Natale, and M. De Rosa, "Frequency comb generation in quadratic nonlinear media," arXiv:1410.6957v1 (2014).
43. A. S. Rogov and E. E. Narimanov, "Frequency comb formation and transition to chaos in microresonators with near-zero dispersion," *Opt. Lett.* **39**, 4305–4308 (2014).
44. H. A. Haus, *Waves and Fields in Optoelectronics* (Prentice-Hall, 1984).
45. W. Suh, Z. Wang, and S. Fan, "Temporal coupled-mode theory and the presence of non-orthogonal modes in lossless multimode cavities," *IEEE J. Quantum Electron.* **40**, 1511–1518 (2004).
46. A. R. Cowan and J. F. Young, "Optical bistability involving photonic crystal microcavities and Fano line shapes," *Phys. Rev. E* **68**, 046606 (2003).
47. E. N. Bulgakov, K. N. Pichugin, A. F. Sadreev, and I. Rotter, "Bound states in the continuum in open Aharonov–Bohm Rings," *JETP Lett.* **84**, 430–435 (2006).
48. N. N. Bogoliubov and Y. A. Mitropolsky, *Asymptotic Methods in the Theory of Non-Linear Oscillations* (Gordon and Breach, 1962).